ROYAL SOCIETY
OF CHEMISTRY

PAPER

Check for updates

Facile fabrication of boron and nitrogen co-doped carbon dots for "ON–OFF–ON" fluorescence sensing of Al³⁺ and F⁻ ions in water samples†

Yahya S. Alqahtani,[a] Ashraf M. Mahmoud,[a] Mater H. Mahnashi,[a] Ramadan Ali,[bc] Reem Y. Shahin,[d] Mohamed M. El-Wekil [ORCID] *[e] and Hany A. Batakoushy[f]

Water contamination with harmful ions has grown to be a significant environmental issue on a global scale. Therefore, the fabrication of simple, cost-effective, and reliable sensors is essential for identifying these ions. Herein, co-doping of carbon dots with new caffeine and H_3BO_3-derived boron (B) and nitrogen (N) was performed (BN@CDs). The as-prepared BN@CDs probe was used for the tandem fluorescence sensing of Al^{3+} and F^- based on "ON–OFF–ON" switches. The BN@CDs nanoswitch has a high quantum yield of 44.8% with $\lambda_{exc.}$ and $\lambda_{em.}$ of 360 nm and 440 nm, respectively. The probe exhibited good stability with different pH, ionic-strengths, and irradiation times. The fluorescence emission of BN@CDs was decreased as the Al^{3+} concentration was increased with a linear range of 0.03–90 μM and a limit of detection (S/N = 3) equal to 9.0 nM. Addition of F^- restored the BN@CDs emission as F^- ions form a strong and stable complex with Al^{3+} ions $[Al(OH)_3F]^-$. Therefore, the ratio response ($F/F°$) was raised by raising the F^- ion concentration to the range of 0.18–80 μM with a detection limit (S/N = 3) of 50.0 nM. The BN@CDs sensor exhibits some advantages over other reported methods in terms of simplicity, high quantum yield, and low detection limit. Importantly, the sensor was successfully applied to determine Al^{3+} and F^- in various ecological water specimens with accepted results.

1. Introduction

Aluminum (Al^{3+}) is usually present in small concentrations in drinking water. The accepted limit of Al^{3+} is below 0.2 mg L^{-1}, according to WHO guidelines.[1] The uptake of Al^{3+} in plasma is carried out by transferrin, which results in the displacement of iron from transferrin and decreases the iron uptake by about 30% with subsequent damage to hemoglobin synthesis.[2] Moreover, elevated levels of Al^{3+} cause Alzheimer's disease, osteomalacia, and dementia.[3] Fluoride (F^-) is naturally

occurring in the soil and groundwater. Increased F^- consumption leads to skeletal and dental fluorosis in both children and adults. It also causes anorexia, gastroenteritis, weakness of muscles, muscle stiffness, dyspnea, sweating, and tachycardia.[4] The conventional methods used for the determination of Al^{3+} and F^- ions are spectrophotometry,[5,6] spectrofluorimetry,[5,7] and atomic absorption spectrometry.[8,9] Some of these methods suffer from low sensitivity and the need for preconcentration steps. In contrast, fluorescence-based methods have gained a lot of attention concerning the sensing capability owing to their simple operation, greater response, and fast detection.[10–13]

Carbon dots (CDs), a carbonaceous nanomaterial, have gained much interest in recent years due to their distinctive features, including water solubility, physical and chemical stability, and ease of surface modification.[14–16] These advantages make CDs excellent candidates for applications in cell imaging, catalysis, drug targeting, biosensing, and energy storage applications.[17–20] The photoluminescence properties of CDs are the most interesting features that broaden their applications in quantitative determination.[21] Wei et al. prepared CDs for the estimation of Al^{3+} ion in water samples; it involves mixing of CDs with Al^{3+}, allowing reacting for 10 min, fluorescence was then measured at $\lambda_{exc.}$ of 360 nm after excitation of the mixture for 15 min.[22] The method suffers from low

[a]Department of Pharmaceutical Chemistry, College of Pharmacy, Najran University, Najran, Saudi Arabia

[b]Department of Pharmaceutical Chemistry, Faculty of Pharmacy, University of Tabuk, Tabuk 71491, Saudi Arabia

[c]Department of Pharmaceutical Analytical Chemistry, Faculty of Pharmacy, Al Azhar University, Assiut Branch, 71526, Egypt

[d]Department of Pharmaceutical Chemistry, Faculty of Pharmacy, Sphinx University, New Assiut City, Assiut, Egypt

[e]Department of Pharmaceutical Analytical Chemistry, Faculty of Pharmacy, Assiut University, Assiut, 71526, Egypt. E-mail: mohamed.elwakeel@pharm.aun.edu.eg; mohamed.mohamoud@ymail.com

[f]Department of Pharmaceutical Analytical Chemistry, Faculty of Pharmacy, Menoufia University, Shebin Elkom, 32511, Egypt

† Electronic supplementary information (ESI) available. See DOI: https://doi.org/10.1039/d3ra02919k

sensitivity and long-time of analysis. A fluorescence sensor for F⁻ ion was fabricated by Liu *et al.* depending on quenching of CDs by F⁻ ion.[23] The optical, electronic, and surface passivation of the CDs can be amended by inserting atoms such S, P, B, and N.[24] The ideal dopants for CDs are S and N as a result of similarity in atomic radius and electronegativity with carbon (C).[25–28]

These facts led to the development of a validated "ON–OFF–ON" fluorescence probe for the detection of fluoride (F⁻) and aluminum (Al³⁺) ions in environmental water samples. The probe is based on innovative B, N@CDs synthesized from caffeine and boric acid. The fluorescence intensity of the probe was quenched by Al³⁺ and recovered by F⁻. The simplicity, acceptable sensitivity, high selectivity, and reliability are only a few of the numerous benefits of the as-created B, N@CDs as it is currently constructed.

2. Experimental

2.1. Materials and reagents

Caffeine (≥98%) was obtained as a gift from NODCAR, Giza, Egypt. Tris–HCl was purchased from Sigma-Aldrich. Boric acid (H_3BO_3, AR), NaOH (AR), HCl (AR), Na_2HPO_4, NaH_2PO_4, and ascorbic acid (AA, ≥97%) were purchased from El-Nasser Co. for intermediate chemicals, Egypt.

2.2. Instrumentation

See ESI.†

2.3. Preparation of BN@CDs

The BN@CDs probe was created using a simple hydrothermal one-step process. Generally, 0.5 g of caffeine, 0.5 g H_3BO_3, and 20 mL of deionized water (DI) were mixed and sonicated for about 5 min. After that, the resultant mixture was heated for 5 h at 180 °C in an oven. Then, the solution was cooled to room temperature (RT). A dialysis bag (3 kDa) was employed to dialyze BN@CDs solution which was then freeze-dried into a solid powder. The un-doped CDs were prepared under the same conditions using 0.5 g of citric acid as a starting material.

### 2.4. Fluorescence sensing for Al³⁺ and F⁻ detection

For Al³⁺, a 300 µL aqueous solution of BN@CDs (0.65 mg mL⁻¹) was added to 1.0 mL phosphate buffered solution of (pH 7.0) and various amounts of Al³⁺. The resultant solution was stood at RT for 2 min and, complete volume to 2 mL with DI. The fluorescence of solutions was measured at $\lambda_{exc.}$ = 440 nm after illumination at 360 nm. For detection of F⁻, 300 µL aqueous solution of BN@CDs (0.65 mg mL⁻¹) was added to 1.0 mL phosphate buffered solution of (pH 7.0) and 100 µL of Al³⁺ (final concentration = 90 µM) before incubation at RT for 2 min. After that, it was mixed with different volumes of F⁻ before completing the volume to 2 mL with DI. The fluorescence spectra were recorded after 1 min (Scheme 1).

2.5. Quantum yield (QY) measurement

Details for calculation of quantum yield were described in ESI.†

2.6. Sample preparations

Potable water from our laboratory, mineral water from local markets, and Nile river water were exposed for the analysis using the proposed fluorimetric method. All samples were analyzed without pretreatment except the Nile river water samples that were filtered using medium sized filter papers.
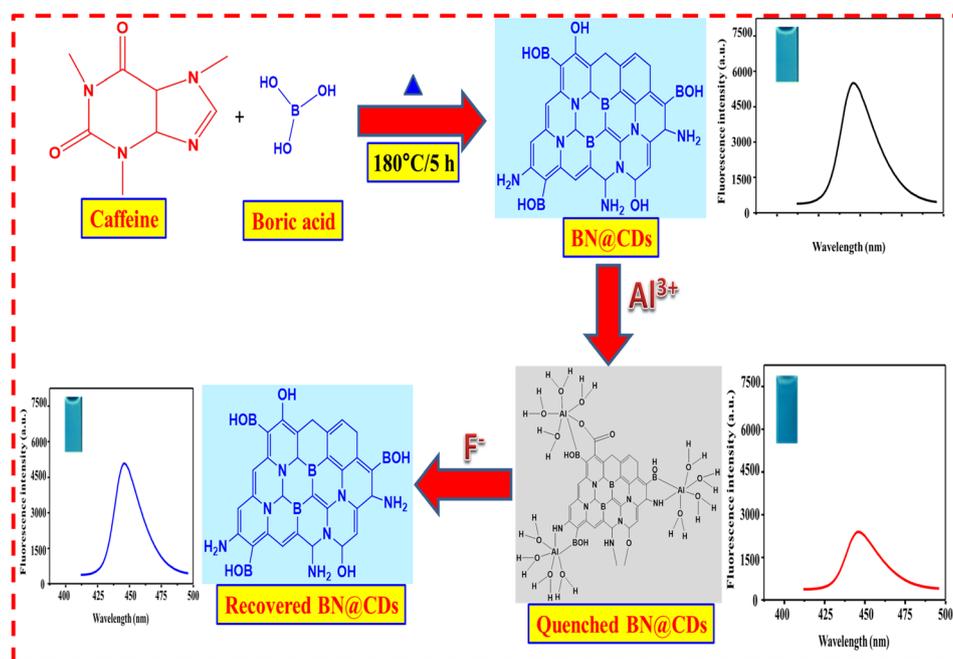
Scheme 1 Preparation of BN@CDs sensor and its utility for Al³⁺ and F⁻ ions determination.

3. Results and discussions

3.1. Characterization

The surface morphology and the average diameter of BN@CDs were investigated using TEM (Fig. 1A). It is well seen that the as-created carbon dots have a rounded shape and homogeneously distributed with no deceptive accumulation. The inset of Fig. 1A exhibits to the HR-TEM of BN@CDs with a lattice spacing of 0.21 nm, referring to the (002) lattice fringes of graphene.[29] Moreover, the average diameter of BN@CDs was calculated to be 4.2 nm (n = 72) (Fig. 1B). The PXRD pattern of BN@CDs was shown in Fig. 1C with a diffraction peak at 23.6°, corresponding to the (002) plane of graphene.[30,31] The FT-IR scan of the proposed probe was investigated in Fig. 1D. The bands at 3380 cm^{-1} refers to the stretching vibrations of OH, NH, and B–OH. Furthermore, sharp peak at 1713 cm^{-1} explores the stretching vibrational band of the carbonyl group. The bands at 1250 cm^{-1} and 1050 cm^{-1} are related to the stretching vibrations of (C–O) and (B–O–B), respectively. Fig. 1E shows the EDX spectrum of BN@CDs with characteristic peaks of B, C, O, and N. Fig. 1F exhibits Raman spectra of BN@CDs and CDs with characteristic bands at 1392 (D-band) and 1593 cm^{-1} (G-band). The D/G ratios of BN@CDs and CDs were calculated as 0.94 and 0.83, respectively, confirming the more defects in carbon nanostructures with BN@CDs than CDs.[32] XPS was employed to investigate the groups functionalizing the surface of BN@CDs (Fig. S1†). Fig. S1a† shows the full XPS spectrum of BN@CDs with the corresponding C 1s, N 1s, O 1s, and B 1s peaks. Fig. S1b† explores the high resolution XPS spectrum (HR-XPS)

of C 1s where it shows bands at 283.3 eV, 284.1 eV, and 285.9 eV, which are assigned to C=C, C–C/C–N, C=O/C=N, respectively. The HR-XPS spectrum of N 1s shows the bands at 396.8 eV, 398.3 eV, 402.2 eV, 406.7 eV, attributable to pyridine N, pyrrolic N, graphitic N, and *N*-oxide form, respectively (Fig. S1c†). Additionally, the HR-XPS spectrum of O 1s was introduced in Fig. S1d† where it shows bands at 529.4 eV, 530.8 eV, and 533.3 eV, which are assigned to C–O, C=O, C–OH/C–O–C, respectively. Fig. S1e† explores the HR-XPS of B 1s with main bands at 190.3 eV, 191.2 eV, 192.4 eV, 195.6 eV, assigning to B–C, B=O, Bi$_2$O$_3$, and B–O, respectively.[33]

The optical characteristics of BN@CDs were studied using spectrophotometry and fluorescence spectroscopy (Fig. 2). The bands at 235 nm and 318 nm in the UV/vis absorption spectrum of BN@CDs are attributed to C=C and C=N/C=O transitions. In addition, the fluorescence spectrum of BN@CDs exhibits an emission peak at 440 nm following illumination at $\lambda_{exc.}$ = 360 nm (Fig. 2a). Variation of excitation wavelengths resulted in shifting the emission wavelengths in the range of 300–400 nm, confirming the variations in the particle sizes of as-fabricated BN@CDs (Fig. 2b). Additionally, the quantum yield of the BN@CDs was calculated at 44.8%, indicating the strong emission of BN@CDs.

3.2. Stability of BN@CDs probe

The influence of different environmental factors regarding on the stability of the probe was investigated in Fig. S2.† The effect of different pH values was studied; it was found that a slight variation in the fluorescence emission was seen in the pH range
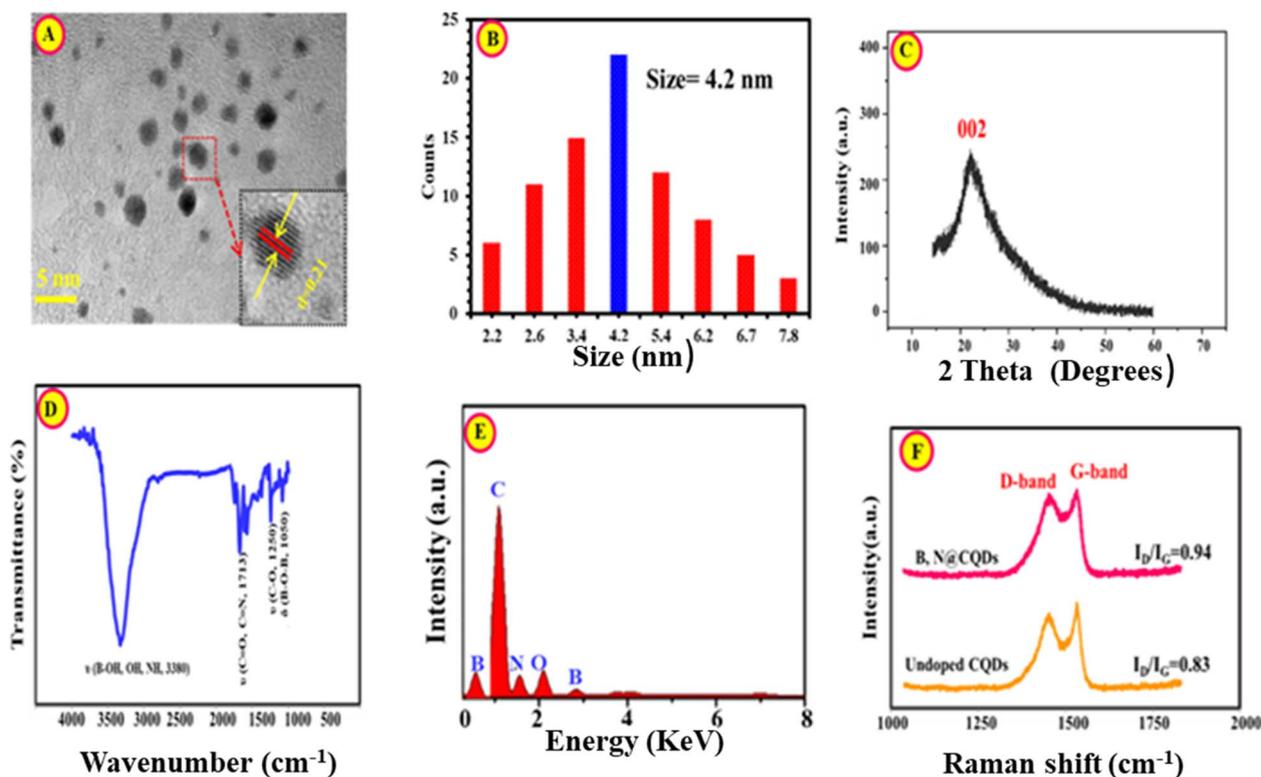

Fig. 1   TEM (A), size distribution diagram (B), PXRD (C), FT-IR (D), and EDX (E) of BN@CDs while (F) is Raman spectra of BN@CDs and CDs.
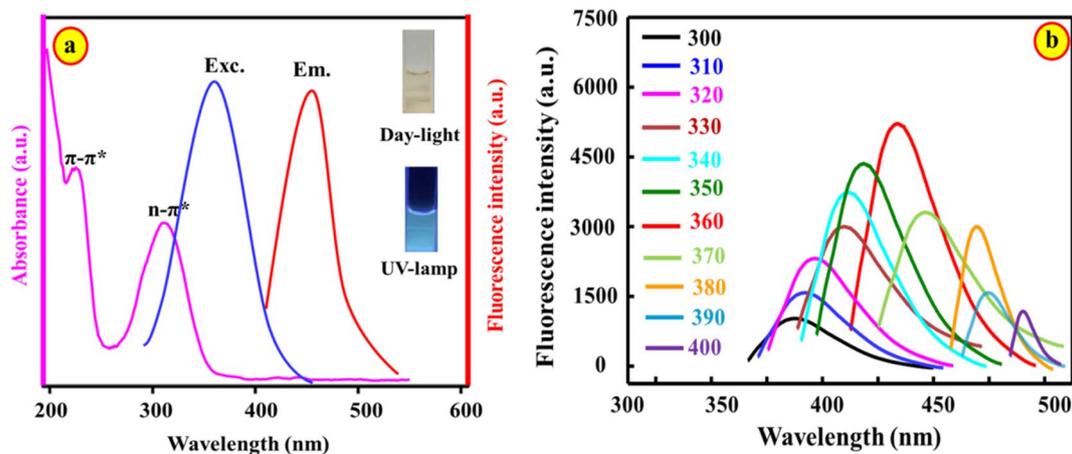
Fig. 2 Absorption and fluorescence spectra of BN@CDs (a); dependency of emission on excitation wavelengths (b).

of 4–10, confirming the high stability of BN@CDs over a wide range of pH values (Fig. S2a†). Moreover, the stability was tested under high ionic strength; it was observed that there was a slight variation in the emission of BN@CDs following the high concentration of ionic strength (Fig. S2b†). Additionally, the stability of the BN@CDs was investigated under UV illumination at 365 nm; it was found that the fluorescence emissions were stable for 120 min, proving the high stability of the BN@CDs after exposure to long-term UV exposure (Fig. S2c†).

3.3. Optimization of variables

3.3.1. Synthesis variables. Parameters affecting the synthesis of the nanoswitch were optimized, including caffeine : H_3BO_3 ratio, synthesis temperature, and heating time (Fig. S3†). It was found that the ratio of caffeine : H_3BO_3 significantly influenced the fluorescence emission and wavelengths of BN@CDs (Fig. S3a†). The maximum emission of BN@CDs was obtained at a ratio of 1 : 1 with a wavelength of 440 nm. When the ratio of caffeine to H_3BO_3 was changed to 2 : 1, the fluorescence emission decreased, while increasing the

amount of H_3BO_3 (caffeine : $H_3BO_3 = 2 : 1$) resulted in lowering the emission intensity with a red-shifted emission spectrum. Moreover, the influences of reaction temperature and heating times were investigated in Fig. S3b and c.† It is seen that the increase in reaction temperature resulted in an improvement in fluorescence emission with a trivial shift in the fluorescence wavelength. A lower temperature was selected that did not affect the fluorescence emission of the BN@CDs. Thus, 180 °C was chosen as an optimum value for subsequent steps. In addition, the optimal heating time was selected as 5 h.

3.3.2. Reaction variables. To improve Al^{3+} ions detection, the experimental variables influencing the detection was optimized (Fig. S4†). Fig. S4a† explores the pH effect on the emission of BN@CDs after the addition of the Al^{3+} ion. It was found that the ratio responses (F^o/F) [F^o and F are the fluorescence emission before and after addition of Al^{3+}] were enhanced with increasing the pH value until the optimum value at 7.0. After this value, the readings were decreased, which may be due to the formation of aluminate (AlO_2^-) at higher pH values.[3] Therefore, pH 7.0 was taken as an optimum value for
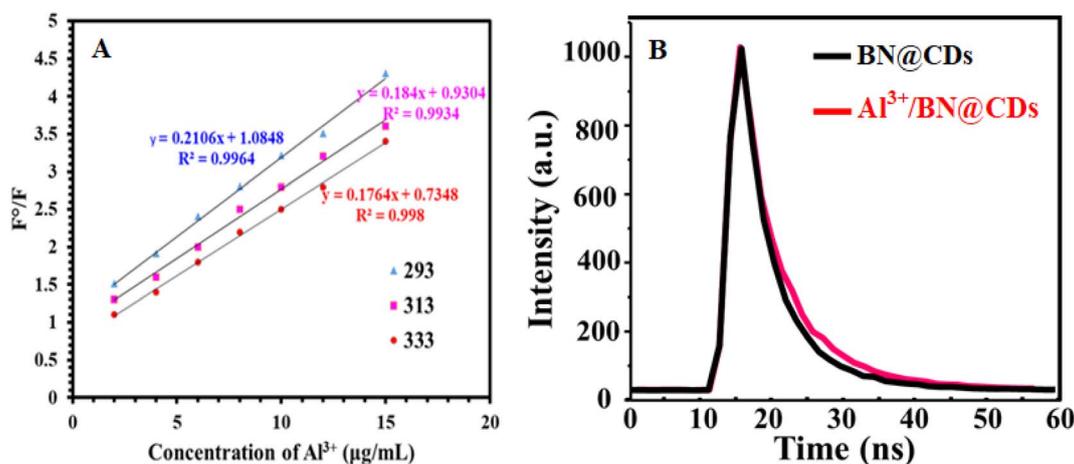

Fig. 3 (A) Stern–Volmer plots of BN@CDs after addition of Al^{3+} at different temperatures. (B) Fluorescence lifetimes of BN@CDs and BN@CDs/Al^{3+}.

subsequent determinations. Moreover, the influence of incubation time was investigated in Fig. S4b.† It was concluded that the readings were increased with increasing the incubation time until 2 min; after that, the response ratio did not significantly change. Therefore, 2 min was used as an ideal reaction time between BN@CDs and Al^{3+}.

3.4. Sensing mechanism and principal of the detection

In order to illustrate the detection mechanism, the interaction between BN@CDs and Al^{3+} was investigated using the Stern–Volmer equation:[24] $F^{o}/F = 1 + K_{SV}Q$ (F^{o} and F are the fluorescence emission of BN@CDs in the presence and absence of Al^{3+}), K_{SV} is the Stern–Volmer constant, and Q is the concentration of Al^{3+}. It was found that the K_{SV} values (slopes) at 333 K, 313 K, and 293 K were 0.211×10^3 g^{-1} L, 0.184×10^3 g^{-1} L, and 0.176×10^3 g^{-1} L, respectively, which confirm static-quenching (Fig. 3A).[34] Moreover, the fluorescence lifetimes of BN@CDs before and after addition of Al^{3+} were found to be 16.23 ns and 16.18 ns, confirming static quenching (Fig. 3B). The quenching of BN@CDs maybe attributed to the interaction between amino groups (Lewis base) on the surface of BN@CDs and Al^{3+} (Lewis acid). The strong coordination complex between the nitrogen and Al^{3+} ions enhances the selectivity of the detection.[35] In addition, the doping of boron (B) improves the coordination between (N) and Al^{3+}, enhancing the coordination complexation and thus improving the detection sensitivity.[36] Moreover, the "Lewis-base" property of (B) enables the coordination interaction between (B) and (Al^{3+}).[37,38] Therefore, BN@CDs could be efficiently applied to detect Al^{3+} ion in different sample matrices with high selectivity. The Al^{3+} ion is reported to produce Al(OH)$_3$F$^-$ in weakly alkaline medium by forming a stronger complex with the F$^-$ ion than all the other metal ions. At a pH of around 7.0, the form Al(OH)$_3$F$^-$ predominates over others.[39] The complex formation between Al^{3+} and F$^-$ ions releases the BN@CDs and restores its fluorescence emission. The fluorescence response of BN@CDs was determined in the presence of F$^-$ ion (Fig. 4A). The studies proved that the fluorescence

response of BN@CDs did not change upon adding F$^-$ ion. These results specify that the anion recognition accomplished by direct use of BN@CDs is not present as a result of electron-rich groups. Therefore, BN@CDs/Al^{3+} probe was designed for indirect fluorometric sensing of F$^-$ ion. Fig. 4B shows the zeta-potentials of BN@CDs, BN@CDs/Al^{3+}, and BN@CDs/Al^{3+}/F$^-$ systems, which are -21.72 mV, $+23.24$ mV, and $+4.88$ mV. The difference in the surface charge density confirmed the interaction between Al^{3+} and F$^-$. Moreover, the fluorescence lifetimes of BN@CDs/Al^{3+} hybrid before and after addition of F$^-$ were investigated (Fig. 4C). The fluorescence lifetime of BN@CDs/Al^{3+} is 15.46 ns, which is increased after addition of F$^-$ to 16.34 ns, suggesting a strong complex formation between BN@CDs/Al^{3+} and F$^-$.

3.5. Calibration plots

Under optimum conditions, fluorescence emission spectra were recorded after incubation of BN@CDs with different
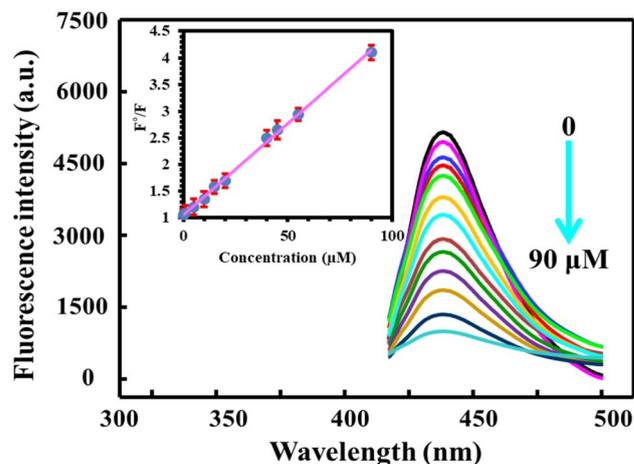

Fig. 5 The influence of different concentrations of Al^{3+} (0–90 μM) on the fluorescence response of BN@CDs under optimum conditions.

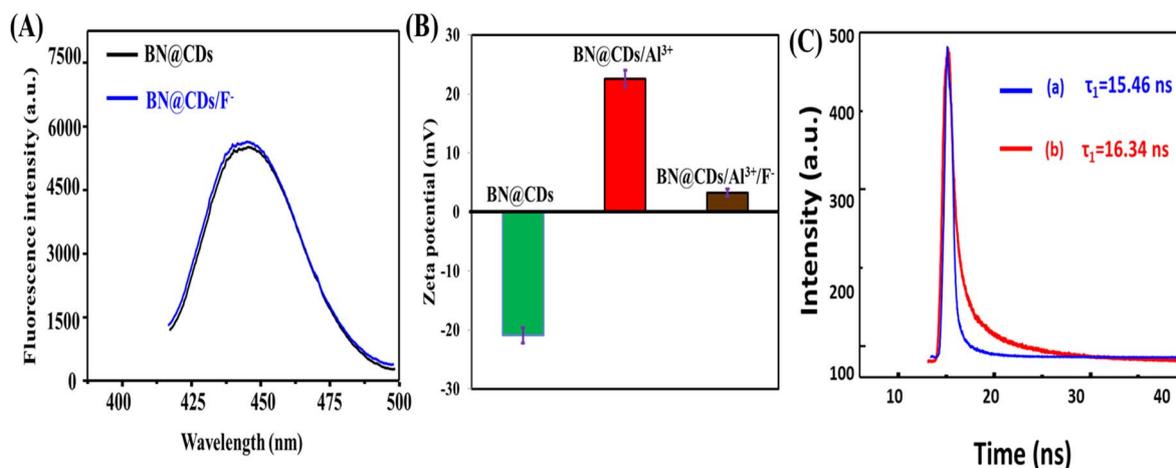

Fig. 4 (A) Fluorescence spectra of BN@CDs and BN@CDs/F$^-$; (B) zeta-potentials of BN@CDs, BN@CDs/Al^{3+}, and BN@CDs, BN@CDs/Al^{3+}/F$^-$; (C) fluorescence lifetimes of Al^{3+}/BN@CDs before (a) and after (b) after addition of F$^-$.
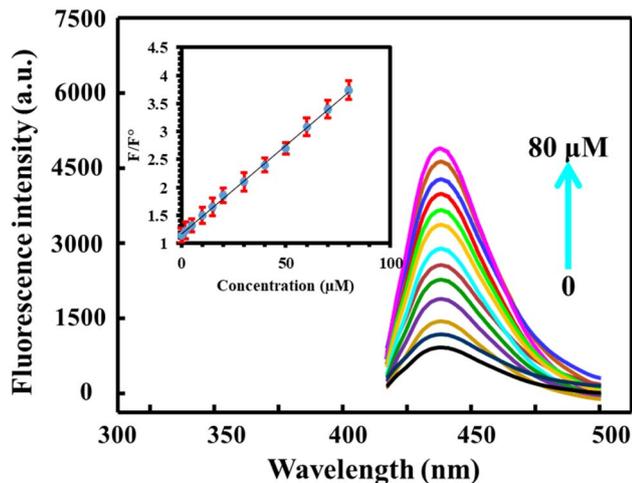
Fig. 6 The influence of different concentrations of F⁻ (0–80 μM) on the fluorescence response of BN@CDs/Al³⁺ system under optimum conditions.

Al^{3+} from 0.03 to 90 μM with a detection limit (S/N = 3) of 9.0 nM. The linear regression equation between F^o/F and concentration of Al^{3+} can be expressed as: $F^o/F = 1.05 + 0.034C_{Al^{3+}} (R^2 = 0.9986)$ (Fig. 5). Interestingly, the addition of F^- recovered the fluorescence of BN@CDs treated with Al^{3+} as a result of strong complexation between Al^{3+} and F^-. Thus, the addition of different amounts of F^- recovered the fluorescence emission again. Fig. 6 explores the recorded fluorescence spectra after the addition of different concentrations of F^- ion in the range of 0.18–80 μM. The response ratios (F/F^o) were increased with the addition of F^- according to the following linear regression: $F/F^o = 0.023 + 0.0114C_{F^-} (R^2 = 0.9988)$ with a detection limit of 5.0 nM. Additionally, the as-fabricated sensor was compared with other reported sensors for the determination of Al^{3+} and F^- ions (Table 1). It was concluded that the proposed sensor exhibited the lowest LOD value and the wide-linear range, proving that the proposed probe can be applied to determine Al^{3+} and F^- in real samples with high sensitivity.

3.6. Reproducibility and selectivity

The reproducibility of BN@CDs was evaluated by measuring the response of the fluorescent probe for four days. The RSD% was

concentrations of Al^{3+}. It is obvious that increasing the amount of Al^{3+} decreases the fluorescence of the probe. Notably, the response ratios increased with increasing the concentration of

Table 1 Quantitative parameters of the created BN@CDs and other functionalized CDs for fluorometric assay of Al^{3+} and F^-

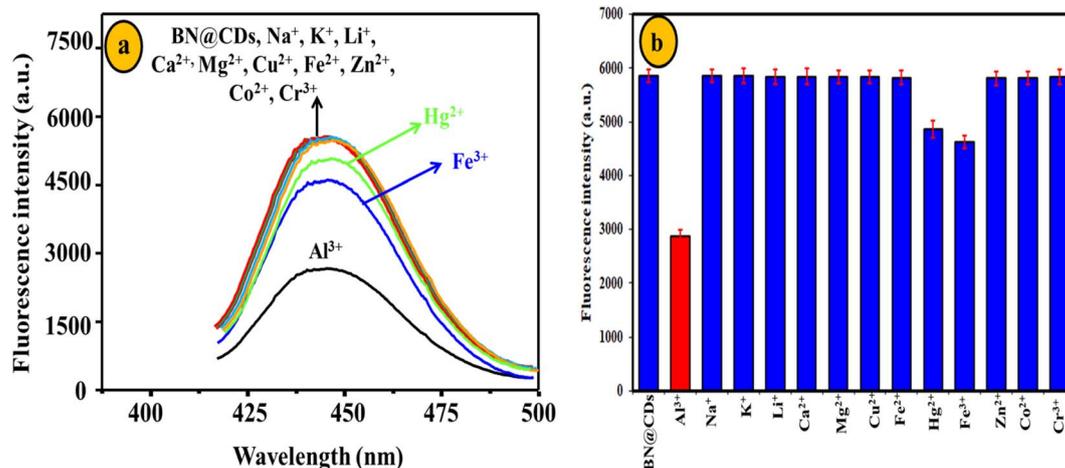| Analyte	Probe	Dynamic linear range (μM)	LOD (μM)	Reference
Al^{3+}	B, N@CDs	0–100	1.07	35
	β-Cyclodextrin–N@CDs	0–20	0.231	40
	Amino acid@CDs	1–20	0.32	41
	N@CDs	10–2500	0.023	42
	N@CDs	0–500	0.216	43
	B, N@CQDs	0–100	1.07	44
	B, N@CDs	**0.03–90**	**0.009**	**This work**
F^-	Se, N@CDs–curcumin	2–60	0.39	45
	N@CDs/Al³⁺–morin complex	0.5–150	2.09	46
	N@CDs/Fe³⁺	0–21	1.26	47
	B, N@CDs/Al³⁺	**0.18–80**	**0.05**	**This work**

Fig. 7 Selectivity of BN@CDs towards 25 μM Al³⁺ in the presence of 300 μM interfering metal cations.
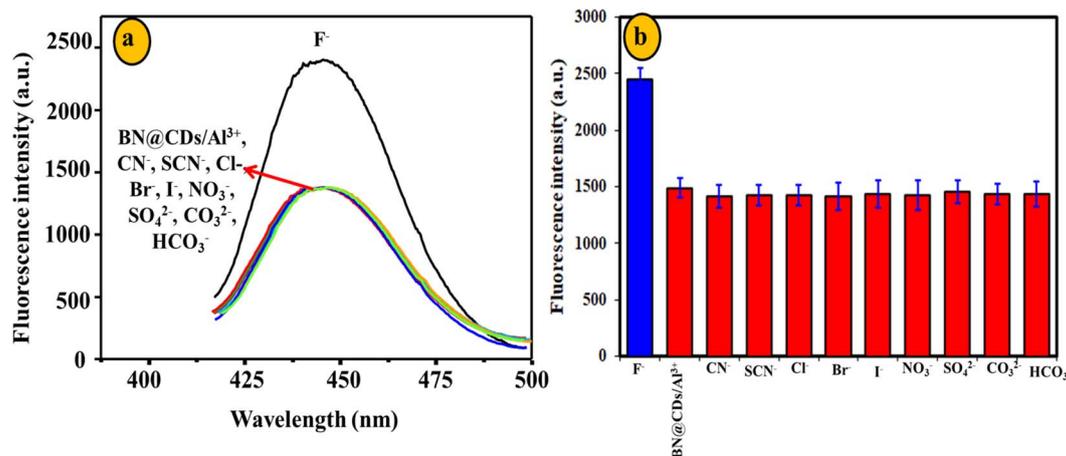
Fig. 8 Selectivity of BN@CDs/Al^{3+} system towards 5 μM F^- in the presence of 100 μM coexisting anions.

Table 2 Application of BN@CDs sensor for the determination of Al^{3+} in water samples

Water sample	Added (μM)	BN@CDs sensor			Reported[46]		
		Found (μM)	Recovery%	RSD%	Found (μM)	Recovery%	RSD%
Tap	2.0	1.98	99.0	2.8	1.96	98.0	3.7
	5.0	5.13	102.6	3.6	4.88	97.6	3.3
	10.0	10.45	104.5	2.9	10.54	105.4	3.7
River	2.0	2.08	104.0	3.0	1.97	98.5	4.0
	5.0	4.95	99.0	3.5	5.25	105.0	4.2
	10.0	9.65	96.5	3.1	9.56	95.6	4.0
Mineral bottled	2.0	1.98	99.0	4.0	2.11	105.5	3.6
	5.0	5.12	102.4	3.5	5.08	101.6	3.7
	10.0	10.35	103.5	2.8	9.57	95.7	3.2

Table 3 Application of BN@CDs/Al^{3+} system for assay of F^- in water specimens

Water sample	Added (μM)	BN@CDs/Al^{3+} system			Reported method[47]		
		Found (μM)	Recovery%	RSD%	Found (μM)	Recovery%	RSD%
Tap	2.0	1.92	96.0	3.2	1.94	97.0	3.4
	5.0	4.87	97.4	3.9	4.85	97.0	3.8
	10.0	9.78	97.8	3.6	10.23	102.3	4.3
River	2.0	1.96	98.0	3.6	2.07	103.5	4.5
	5.0	4.94	98.8	3.9	5.13	102.6	2.9
	10.0	10.50	105.0	3.6	9.56	95.6	4.4
Mineral bottled	2.0	2.03	101.5	2.8	1.97	98.5	3.1
	5.0	4.97	99.4	3.3	5.03	100.6	3.0
	10.0	9.78	97.8	3.2	10.45	104.5	3.8

calculated as 3.4%, assuring the reproducibility of BN@CDs approach (Fig. S5a†). Furthermore, reproducibility of the BN@CDs/Al^{3+} probe towards the measurement of F^- was investigated by recording the fluorescence response through four days. The RSD% was estimated as 3.7%, proving the efficiency of the as-prepared probe for the assay of F^- (Fig. S5b†). The selectivity of the sensing probe is an important parameter to evaluate its potential applications. Therefore, the BN@CDs sensor was applied to determine Al^{3+} in the presence of coexisting species such as Na^+, K^+, Li^+, Ca^{2+}, Mg^{2+}, Cu^{2+}, Fe^{2+}, Zn^{2+},

Co^{2+}, and Cr^{3+}. It was found that 300 μM of these interfering cations had an insignificant effect on the response of B, N@CDs, confirming the good selectivity of the as-synthesized probe towards Al^{3+} detection (Fig. 7). It is noteworthy to mention that the major interfering metal cations for Al^{3+} determination are Fe^{3+} and Hg^{2+}, which can be eliminated by addition of ascorbic acid to reduce them to less interfering Fe^{2+} and Hg^{2+}, respectively. Thus, 1.5 mM ascorbic acid was used to eliminate the interference of Fe^{3+} and Hg^{2+} during water samples determination. Additionally, the selectivity of the

BN@CDs/Al^{3+} probe towards the assay of F$^-$ was evaluated in the presence of interfering anions such as CN$^-$, SCN$^-$, Cl$^-$, Br$^-$, I$^-$, NO$_3^-$, SO$_4^{2-}$, CO$_3^{2-}$, and HCO$_3^-$ (Fig. 8). It is obvious that only F$^-$ anion can recover the fluorescence emission of the probe, confirming the good selectivity of the as-prepared system towards F$^-$ detection.

3.7.   Applications of BN@CDs sensor and BN@CDs/Al^{3+} system

The BN@CDs sensor and BN@CDs/Al^{3+} system were applied to determine the amount of Al^{3+} and F$^-$ in water samples, respectively (Tables 2 and Table 3). It was found that the recoveries% of Al^{3+} and F$^-$ in different water samples are 96.5–104.5% and 96.0–105.0% with LOD values did not exceed 4.0 and 3.9%, respectively, confirming the accuracy of the sensor for the assay of Al^{3+} and F$^-$. When the obtained findings were compared to those of the reported methods, it was discovered that the results were generally in agreement, indicating that the suggested sensor/system is accurate.

4.   Conclusion(s)

A novel fluorescent probe based on BN@CDs was fabricated from caffeine and H$_3$BO$_3$ using a facile hydrothermal method. The as-synthesized BN@CDs exhibited good stability under a variety of conditions, including different irradiation times, pH, and ionic strength. The strong fluorescence emission of the BN@CDs was utilized to detect Al^{3+} and F$^-$ ions. The addition of Al^{3+} ions quenched the emission of BN@CDs *via* the static mechanism. The quenched response of the BN@CDs/Al^{3+} system was further used to estimate the amount of F$^-$ ion. The fluorescence emission of BN@CDs was regenerated after addition of F$^-$ as a result of coordination interactions between Al^{3+} and F$^-$ forming an Al(OH)$_3$F$^-$ stable complex. The BN@CDs sensor and BN@CDs/Al^{3+} system exhibited many advantages, including a low detection limit, good selectivity, reproducibility, and reliability. Additionally, the sensor/system was efficiently applied to determine Al^{3+} and F$^-$ ions in various watery specimens with accepted results.

Conflicts of interest

The authors declare that they have no known competing financial interests or personal relationships that could have appeared to influence the work reported in this paper.

Acknowledgements

References

1 World Health Organization, *Guidelines for drinking-water quality, incorporating 1st and 2nd addenda recommendations*, World Health Organization, Geneva, 3rd edn, 2008, p. 1.

2 N. A. Gomez, A. S. Lorenzetti, J. Camiña, M. Garrido and C. E. Domini, *Microchem. J.*, 2022, **183**, 108117.

3 B. A. Alyami, A. M. Mahmoud, S. A. Alkahtani and M. M. El-Wekil, *Talanta*, 2021, **226**, 122167.

4 A. M. Mahmoud, M. H. Mahnashi, S. S. Abu-Alrub, S. A. Alkahtani and M. M. El-Wekil, *J. Electrochem. Soc.*, 2021, **168**, 126525.

5 O. Domínguez-Renedo, A. M. Navarro-Cuñado, E. Ventas-Romay and M. A. Alonso-Lomillo, *Talanta*, 2019, **196**, 131–136.

6 B. Yardımcı, A. Üzer and A. Üzer, *ACS Omega*, 2022, **7**, 45432–45442.

7 H. Abdolmohammad-Zadeh, Z. Rezvani, G. H. Sadeghi and E. Zorufi, *Anal. Chim. Acta*, 2011, **685**, 212–219.

8 M. A. Qadir, M. Ahmed and S. Shahzad, *Anal. Lett.*, 2015, **48**, 147–153.

9 A. Dhillon, M. Nair and D. Kumar, *Anal. Methods*, 2016, **8**, 5338–5352.

10 H. B. Wang, B. B. Tao, N. N. Wu, H. D. Zhang and Y. M. Liu, *Spectrochim. Acta, Part A*, 2022, **271**, 120948.

11 H. B. Wang, B. B. Tao, A. L. Mao, Z. L. Xiao and Y. M. Liu, *Sens. Actuators, B*, 2021, **348**, 130729.

12 H. Zhang, S. Wu, Z. Xing and H. B. Wang, *Analyst*, 2021, **146**, 7250–7256.

13 H. Zhang, S. Wu, Z. Xing, M. Gao, M. Sun, J. Wang and H. B. Wang, *Appl. Phys. A: Mater. Sci. Process.*, 2022, **128**, 356.

14 R. M. K. Mohamed, S. H. Mohamed, A. M. Asran, I. H. Alsohaimi, H. M. A. Hassan, H. Ibrahim and M. M. El-Wekil, *Spectrochim. Acta, Part A*, 2023, **293**, 122444.

15 H. R. H. Ali, A. I. Hassan, Y. F. Hassan and M. M. El-Wekil, *Anal. Bioanal. Chem.*, 2020, **412**, 353–1363.

16 H. R. H. Ali, A. I. Hassan, Y. F. Hassan and M. M. El-Wekil, *Microchim. Acta*, 2019, **186**, 850.

17 A. O. Alqarni, S. A. Alkahtani, A. M. Mahmoud and M. M. El-Wekil, *Spectrochim. Acta, Part A*, 2021, **248**, 119180.

18 H. R. H. Ali, A. I. Hassan, Y. F. Hassan and M. M. El-Wekil, *J. Environ. Chem. Eng.*, 2021, **9**, 105078.

19 H. R. H. Ali, A. I. Hassan, Y. F. Hassan and M. M. El-Wekil, *Food Chem.*, 2021, **349**, 129160.

20 A. M. Mahmoud, M. H. Mahnashi, A. Al Fatease, M. A. H. Mostafa, M. M. El-Wekil and R. Ali, *J. Food Compos. Anal.*, 2022, **108**, 104428.

21 A. M. Mahmoud, M. M. El-Wekil, R. Ali, H. A. Batakoushy and R. Y. Shahin, *Microchim. Acta*, 2022, **189**, 183.

22 W. Wei, J. Huang, W. Gao, X. Lu and X. Shi, *Chemosensors*, 2021, **9**, 25.

23 S. Liu, Z. Liu, Q. Li, H. Xia, W. Yang, R. Wang, Y. Li, H. Zhao and B. Tian, *Spectrochim. Acta, Part A*, 2021, **246**, 118964.

24 Y. S. Alqahtani, A. M. Mahmoud and M. M. El-Wekil, *Talanta*, 2023, **253**, 124024.

25 A. M. Mahmoud, M. H. Mahnashi, F. M. Alshareef and M. M. El-Wekil, *Microchem. J.*, 2023, **187**, 108430.

26 M. H. Mahnashi, A. M. Mahmoud, S. A. Alkahtani and M. M. El-Wekil, *J. Alloys Compd.*, 2021, **871**, 159627.

27 A. M. Mahmoud, S. S. Abu-Alrub, A. O. Alqarni, M. M. El-Wekil and A. B. H. Ali, *Microchem. J.*, 2023, **191**, 108929.

28 K. Alhazzani, A. Z. Alanazi, A. M. Alaseem, S. A. Al Awadh, S. A. Alanazi, A. A. AlSayyari, M. M. Alanazi and M. M. El-Wekil, *Microchem. J.*, 2023, **190**, 108666.

29 A. M. Mahmoud, M. H. Mahnashi, S. A. Alkahtani and M. M. El-Wekil, *Int. J. Biol. Macromol.*, 2020, **165**(part B), 2030–2037.

30 S. A. Alkahtani, A. M. Mahmoud, M. H. Mahnashi, A. O. AlQarni, Y. S. A. Alqahtani and M. M. El-Wekil, *Microchem. J.*, 2021, **164**, 105972.

31 M. H. Mahnashi, A. M. Mahmoud, A. Z. Alanazi, K. Alhazzani, S. A. Alanazi, M. M. Alanazi and M. M. El-Wekil, *Microchem. J.*, 2021, **164**, 106020.

32 X. L. Guo, Z. Y. Ding, S. M. Deng, C. C. Wen, X. C. Shen, B. P. Jiang and H. A. Liang, *Carbon*, 2018, **134**, 519–530.

33 W. Li, L. Zhang, N. Jiang, Y. Chen, J. Gao, J. Zhang, B. Yang and J. Liu, *Molecules*, 2022, **27**, 6771.

34 Y. Wang, Q. Yue, L. Tao, C. Zhang and C. Li, *Microchim. Acta*, 2018, **185**, 550.

35 X. Li, L. Zhao, Y. Wu, A. Zhou, X. Jiang, Y. Zhan and Z. Sun, *Spectrochim. Acta, Part A*, 2022, **282**, 121638.

36 A. M. Bates, W. F. Paxton, J. M. Spurgeon, S. D. Park and M. K. Sunkara, *Appl. Energy*, 2021, **282**, 116252.

37 D. Franz and S. Inoue, *Chem.–Eur. J.*, 2019, **25**, 2898–2926.

38 A. Hofmann, C. Pranckevicius, T. Tröster and H. Braunschweig, *Angew. Chem., Int. Ed.*, 2019, **58**, 3625–3629.

39 R. B. Martin, *Coord. Chem. Rev.*, 1996, **149**, 23–32.

40 M. Yao, J. Huang, Z. Deng, W. Jin, Y. Yuan, J. Nie, H. Wang, F. Du and Y. Zhang, *Analyst*, 2020, **145**, 6981–6986.

41 J. Xu, Y. Zang, F. Yan, J. Sun, Y. Zhang and C. Yi, *Part. Part. Syst. Charact.*, 2021, **38**, 2100201.

42 C. Yan, L. Guo, X. u. Shao, Q. i. Shu, P. Guan, J. Wang, X. Hu and C. Wang, *Anal. Bioanal. Chem.*, 2021, **413**, 3965–3974.

43 X. Mei, D. Wang, L. Zhang, J. Li and C. Dong, *Luminescence*, 2021, **36**, 1469–1475.

44 J. Wu, Y. Zhang, Y. Dong, S. Zhi, X. Yang and C. Yao, *ChemistrySelect*, 2021, **6**, 2966–2974.

45 X. Zhang, X. Tan and Y. Hu, *J. Hazard. Mater.*, 2021, **411**, 125184.

46 Y. Hao, W. Dong, Y. Liu, X. Wen, S. Shuang, Q. Hu, C. Dong and X. Gong, *J. Hazard. Mater.*, 2022, **439**, 129596.

47 S. Kainth, N. Goel, S. Basu and B. Maity, *New J. Chem.*, 2022, **46**, 686–694.